BBA - Biomembranes 1863 (2021) 183468

Contents lists available at ScienceDirect

BBA - Biomembranes

journal homepage: www.elsevier.com/locate/bbamem

Actin networks regulate the cell membrane permeability during electroporation

Aswin Muralidharan[a], Lea Rems[b,c], Michiel T. Kreutzer[a], Pouyan E. Boukany[a,*]

[a] Department of Chemical Engineering, Delft University of Technology, van der Maasweg 9, 2629 HZ Delft, the Netherlands
[b] Department of Applied Physics, Science for Life Laboratory, KTH Royal Institute of Technology, 171 65 Solna, Sweden
[c] Faculty of Electrical Engineering, University of Ljubljana, Trzaska 25, 1000 Ljubljana, Slovenia

ARTICLE INFO

Keywords:
Electroporation
Electropermeabilization
Actin networks
Energy barrier
Temperature dependent kinetics of electroporation

ABSTRACT

Transient physical disruption of cell membranes by electric pulses (or electroporation) has significance in biomedical and biological applications requiring the delivery of exogenous (bio)molecules to living cells. We demonstrate that actin networks regulate the cell membrane permeability during electroporation. Disruption of actin networks increases the uptake of membrane-impermeable molecules such as propidium iodide during electroporation. Our experiments at different temperatures ranging from 11 °C to 37 °C show that molecular uptake during electroporation increases with temperature. Furthermore, by examining the temperature-dependent kinetics of propidium iodide uptake, we infer that the activation energy barrier of electroporation is lowered when the actin networks are disrupted. Our numerical calculations of transmembrane voltage show that the reduced activation energy barrier for the cells with disrupted actin is not a consequence of the changes in transmembrane voltage associated with changes in the cell shape due to the disruption of actin, indicating that this could be due to changes in membrane mechanical properties. Our results suggest that the current theoretical models of electroporation should be advanced further by including the contributions of the cytoskeletal networks on the cell membrane permeability during the delivery of exogenous materials.

1. Introduction

Cell membranes, which are composed of a lipid bilayer with embedded proteins, act as a protective barrier that separates the intracellular components from the extracellular environment. In mammalian cells, the membrane is stabilized by the cytoskeletal network present inside the cell, which is a network of different filamentous biopolymers, including actin fibers and microtubules [1,2]. While the protective function of the membrane is necessary for the survival of the cell, deliberate permeabilization of the cell membrane to deliver exogenous materials such as small drug molecules, nucleic acids, or proteins is often required for biomedical applications [3]. One of the most common and safest non-viral methods used to transiently increase the cell membrane permeability is the introduction of transient transmembrane pores by subjecting the cell to a pulsed electric field [4,5]. This process is called electroporation or electropermeabilization, with applications including DNA vaccination, electrochemotherapy, and irreversible electroporation for nonthermal ablation of solid tumors and cardiac muscle ablation [6–12].

Exposing living cells to electric field results in the build-up of a transmembrane voltage (V_m) [13,14], which promotes the nucleation of electropores (or defects) in the cell membrane [15–19]. When the electric field is removed, the membrane discharges resulting in a gradual recovery (resealing) of the cell membrane to its initial impermeable state [13]. Evidence of the existence of the electropores comes primarily from experiments [20–23] and numerical simulations performed on simplified cell membrane systems composed of lipid bilayers [24–26]. Theory and evidence from experiments and numerical simulations have proposed that the initiation and closure of the electropores are temperature-dependent processes, and are governed by activation energy barriers; the reported values of activation energy barriers of pore creation range between 10 and 45 k_BT where k_B is the Boltzmann constant, and T is the temperature [16,17,21,26–28]. While the lipid bilayer provides an excellent experimental model for studying electroporation, observations from experiments on living cells are often inconsistent with the experiments on simplified lipid bilayer models [13]. In particular, the measured resealing time of electroporated membranes of cells is in the order of several seconds to minutes [29,30] while the resealing time of lipid bilayers is considerably shorter (less than 1 s) [5,23,31]. Besides, the electroporation of giant unilamellar vesicles or

* Corresponding author.
E-mail address: p.e.boukany@tudelft.nl (P.E. Boukany).

https://doi.org/10.1016/j.bbamem.2020.183468
Received 30 May 2020; Received in revised form 14 August 2020; Accepted 26 August 2020
Available online 31 August 2020

GUVs leads to the formation of pores in the size range of micrometers in the membrane (also called macropores) whereas pores of such dimensions are not observed in living cells [22,23,32].

Since the experiments with simplified lipid bilayer models are insufficient to explain all the observations made in living cells, groups have begun to employ a bottom-up approach by investigating artificial cell models with increasing complexity, including multi-component membranes with lipid phase separation [33–35], and GUVs with incorporated cytoskeleton networks [36]. Experiments with GUVs made of gel phase lipids with mechanical and rheological properties several orders of magnitude higher than those of vesicles made of fluid phase lipids show that the voltage required to form pores in the former is several times higher than the latter [33]. When GUVs made with a mixture of fluid and gel phase lipids were electroporated, the electropores form in the fluid phase [34]. The addition of transmembrane proteins like α-hemolysin showed up to a four-fold increase in the voltage required to create pores on 1,2-diphytanoyl-sn-glycero-3-phosphocholine (DPhPC) membranes [35]. The addition of cholesterol altered the minimum voltage required to form pores in the DPhPC membrane depending on the concentration of cholesterol added; concentrations below 5% w/w displayed an increase of approximately 25%, followed by almost a 100% decrease in the voltage required for electroporation at higher concentrations [35]. For GUVs incorporated with actin networks, experiments suggest that upon application of an electric pulse the resealing time of the membrane is longer compared to pure lipids vesicles, and macropores that were observed in empty GUVs were absent in vesicles incorporated with actin networks [36].

Similar to experiments with GUVs with encapsulated cytoskeletal networks, experiments on living cells utilizing chemicals that destabilize the cytoskeletal proteins suggest that the cytoskeleton can address some of the mismatches in observations from lipid vesicles and living cells [37,38]. When Chinese Hamster Ovary (CHO) cells treated with colchicine, a drug that induces microtubule depolymerization, were electroporated (using ten 100 μs pulses of 1.8 kV/cm), ~10% of the treated cells remain permeable 5 min after application of pulses compared to ~60% of the control cells which remain permeable 5 min after delivery of the pulses [37,38]. Furthermore, the application of multiple 100 μs pulses with an amplitude between 100 V/cm and 1200 V/cm to endothelial cells and CHO cells alters the organization of microtubules and actin filaments [39,40]. Moreover, the application of eight 5 ms pulses of 400 V/cm results in a 40% reduction in Young's modulus of CHO cells, which is associated with a destabilized cytoskeleton [41]. Disruption of actin networks in Jurkat cells using latrunculin results in a reduction of the relative proportion of liquid-ordered compared to the liquid-disordered domains in the membrane [42], and experiments on droplet interface bilayers [20] and molecular dynamics simulations [43] show that the electropores form preferentially in the liquid-disordered phase of the membrane. These studies show that the actin networks can influence the permeability of the cells during electroporation and, as a consequence, the delivery of molecules to cells [44]. Recently, experiments have suggested that the disassembly of actin networks inside cells using cytochalasin results in reduced uptake of tracer molecules during electroporation [45]. However, this study has utilized multiple electric pulses, which complicates the interpretation of results from a mechanistic perspective to address the pore formation and closure in the cellular membrane with or without the actin networks. That is because the first pulse can increase the permeability of the cell membrane, and the subsequent pulses can begin disrupting the actin network due to electric currents that can flow through the permeabilized cells [36,46].

Despite several pieces of evidence pointing towards the involvement of cytoskeletal networks in electroporation, the details of how the presence of actin networks influences the permeability of cells during electroporation remain unclear. In this article, we focus on the electroporative uptake of impermeable tracer molecules (propidium iodide) to CHO cells with an intact and disrupted actin filaments when they are exposed to a single electric pulse. We demonstrate that the CHO cells with disrupted actin filaments become more permeable compared to cells with intact actin filaments. By theoretically analyzing our measurements performed at different temperatures, we further demonstrate that the increased membrane permeability in cells with disrupted actin networks can be attributed to reduced activation barrier for pore formation. As such, our combined experimental and numerical results indicate that the presence of actin networks increases the energy barrier of pore formation, possibly due to changes in membrane mechanical properties such as bending modulus.

2. Materials and methods

2.1. Cell culture for electroporation

The Chinese Hamster Ovary cells, CHO-K1 (DSMZ), were grown in T-flasks containing culture medium consisting of Nutrient Mixture Ham F-12 (Sigma Aldrich) supplemented with ~10% Fetal Bovine Serum (Sigma Aldrich) and ~1% Antibiotic-Antimycotic solution (Gibco). The cells were then incubated at 37 °C with 5% CO_2 and were sub-cultured every two days. Twenty-four hours before the electroporation experiments, 1×10^4 cells suspended in 500 μl of culture medium were plated in one well of a four-well glass-bottom chambered coverslip (μ-slide, Ibidi) with a growth area per well of 2.5 cm^2.

2.2. Disruption of actin networks by latrunculin B treatment

To depolymerize the actin filaments, latrunculin B, a marine toxin which binds to a monomer of actin and depolymerizes the actin filaments was used [47,48]. 1 mg of latrunculin B (Enzo Life Sciences, molecular weight: 395.5 g/mol) was purchased as a lyophilized solid and was dissolved in DMSO to obtain a stock solution with a concentration of 25 mg/ml or 63 mM. The stock solution was then stored at a temperature of −20 °C. The stock solution was diluted to a concentration of 0.5 μM in the culture medium on the day of the experiment. We use a concentration of latrunculin B which can cause severe disruption of the actin filaments in the cells [47]. The measured cell viability after latrunculin B treatment is ~100%. The culture medium from the four-well chambered coverslips containing the plated cells was then replaced with 500 μl of 0.5 μM latrunculin B solution. The chambered coverslips were then placed in the incubator for 1 h after which the electroporation experiments were performed.

It was observed that the cells take a spherical morphology as a result of the disruption of the actin filaments compared to their initial flat elongated shapes after the treatment (see Fig. 1(a)). The cells were fixed in 500 μl of 3.7% formaldehyde solution in phosphate buffer saline (PBS) for 5 min to visualize the actin filaments. After this, the cells were washed thrice with 500 μl of PBS. 0.1% Triton X-100 in PBS was then used to permeabilize the cells. The cells were again washed thrice with 500 μl of PBS. The actin filaments of the cells were then stained with 200 μl of 50 μg/ml phalloidin-FITC (Sigma-Aldrich, excitation: 495 nm/emission: 520 nm) solution in PBS by incubating the cells with phalloidin-FITC for 40 min at room temperature (22 °C). The cells were again washed thrice with PBS and imaged under a confocal microscope (Zeiss LSM 710) with a 40×/1.3 oil immersion objective. Fig. 1(a) shows that the control cell displays a network of actin stress fibers while they were absent in the cells treated with latrunculin B.

2.3. Electroporation of CHO cells

The chambered coverslip containing the CHO cells was taken out of the incubator, and the culture medium was removed from the chamber approximately 10 min before the experiment. The cells were then washed three times with 500 μl of pulsing buffer (10 mM Na_2HPO_4/KH_2PO_4, 1 mM $MgCl_2$, 250 mM sucrose, pH 7.0 − 7.4). 500 μl of propidium iodide or PI (Invitrogen) of suitable concentration diluted in the

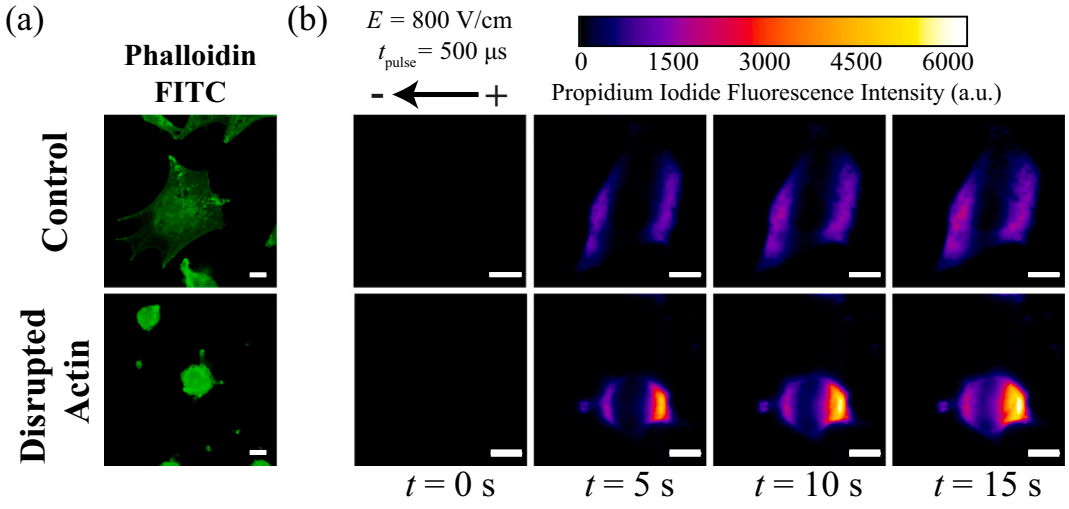

Fig. 1. (a) Representative confocal images showing the structure of the actin network inside the control cells (top) and the cells treated with 0.5 μM latrunculin B to disrupt actin networks (bottom). The cells were fixed in formaldehyde and stained with phalloidin FITC. The images are obtained by using the same imaging settings. (b) Representative fluorescence intensity profiles (bound propidium signal) for CHO cells with intact actin network (top row), and disrupted actin network using 0.5 μM latrunculin B (bottom row) at different times after electroporation (corresponding video file is provided as Supplementary information). No intracellular PI fluorescence was detected before electroporation at $t = 0$ s for both control and treated cells. A single electric pulse with an amplitude of 800 V/cm and a pulse duration of 500 μs was applied for these uptake experiments. The experiments are performed at room temperature (22 °C). Scale bars represent 10 μm.

pulsing buffer was then added to the chambers. Unless otherwise stated, the concentration of PI used in the experiments is 100 μM. PI (molecular weight: 668 g/mol) is a small fluorescent molecule (excitation: 535 nm/emission: 617 nm), which dissociates into propidium ion and iodide ion when dissolved in water and is impermeable to cells with intact membranes [49]. The ions can enter the cells through the electropermeabilized membrane and bind to the nucleic acids present inside the cell, thereby increasing their fluorescence intensity.

The chambered glass slide was then placed on a Linkham PE94 temperature-controlled stage for 10 min, which allows the cells to attain the required temperature. The temperature inside the chambered glass side was measured using a thermocouple (type K, Ibidi). The temperature of the stage was set to be 4 °C, 22 °C, 35 °C, or 44 °C so that the sample attains a temperature of 11 °C, 22 °C, 28 °C, or 37 °C respectively. For the experiments which require cooling, the stage was supplied with demineralized water at room temperature using an aquarium pump (Eheim). The electric field was applied to the cells using custom made stainless steel electrodes placed parallel to each other with 3 mm spacing, which were inserted inside the imaging chamber such that the electrodes were positioned at the bottom of the coverslip. For this electrode geometry, we calculate the electric field experienced by the cells as the voltage to distance ratio. The electrodes were connected to a pulse generator (BETA tech) to deliver the electric pulses. The imaging chamber was positioned on an inverted fluorescence microscope in such a way that cells which look morphologically healthy were in the field of view. Unless stated otherwise, the applied voltage drop across the electrodes was 240 V, corresponding to an electric field of 800 V/cm. Only one pulse with a duration of 500 μs is applied during all the experiments. This pulsing condition is expected to result in negligible temperature increase (~0.1 K) due to Joule heating (see Supplementary information Section S8).

2.4. Fluorescence imaging and analysis of propidium iodide uptake

The fluorescence imaging experiments were performed on an inverted fluorescence microscope (Zeiss Axio-Observer Z1) coupled with an EMCCD camera (Andor ixon3) with a resolution of 512 × 512 pixels. A 100×/1.2 oil immersion objective (Zeiss Acroplan) was used for magnification resulting in a field of view of 81.92 × 81.92 μm^2. An HXP 120C lighting unit (Zeiss) coupled with a Texas red filter set (excitation: 538 nm/emission: 617 nm) was used as a light source for fluorescence imaging of uptake of PI. Acquisition of a series of images (14 bit) with an exposure time of 20 ms with a 52 ms interval, resulting in a frequency of 19.15 frames per second was initiated approximately 10 s before the pulse.

3. Results

3.1. Disruption of actin networks results in increased uptake of propidium iodide during electroporation

To measure the uptake of small molecules to the cells after electroporation, we use a membrane-impermeable molecule, PI, as a marker molecule. Propidium ions emit a strong fluorescence signal when they bind to nucleic acids, which are present inside the cell. Hence, when an electric pulse is applied to the cell in the presence of PI, an increase in fluorescence intensity is observed as a result of transport of the propidium ions to the cell through the permeabilized cell membrane [50]. The uptake of propidium ions by cells during electroporation for an experiment where a single 500 μs pulse with an amplitude of 800 V/cm is applied at room temperature is displayed in Fig. 1(b) (the uptake profiles at lower magnification providing a larger field of view is presented in Supplementary information Fig. S3). The transport of propidium ions follows two stages. During the electric pulse, the propidium ions are electrophoretically delivered to the cells from the side facing the positive electrode. After the pulse, the propidium ions continue to diffuse through the permeabilized membrane from both sides of the cell facing the electrodes until the membrane recovers it's selective permeability (time scale ~10 s) [50,51]. This results in increased fluorescence intensity at both poles of the cell as seen in Fig. 1(b).

The time-series images are analyzed to extract the increase in fluorescence intensity inside the cell with time after the electric pulse is applied using a customized script, coded in Matlab®. First, a region of interest is selected by manually outlining the individual cells. The intensity of an image before electroporation is subtracted from all the images to remove the background signal. The sum of the intensity values in the region of interest is then divided by the number of pixels inside the region of interest for each frame to obtain the transient fluorescence intensity profiles (I_{Total}). The time corresponding to 0 s is defined as the frame in which an increase in fluorescence intensity

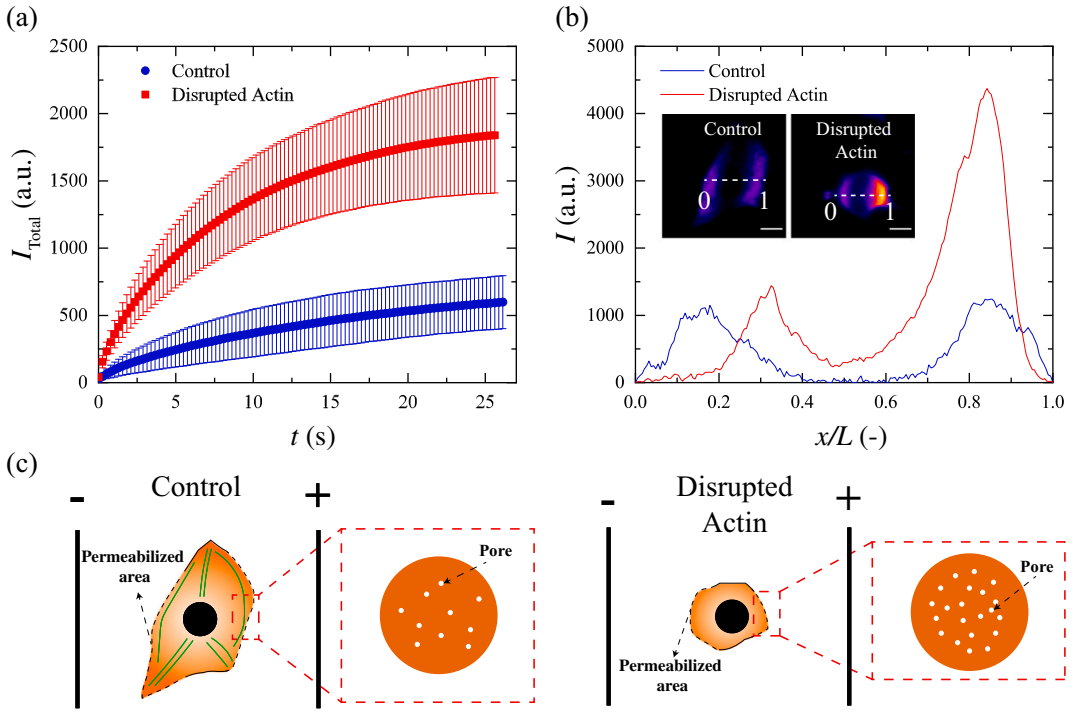

Fig. 2. (a) Temporal evolution of the total fluorescence intensity divided by the number of pixels in the region of interest both the control cells and the treated cells at room temperature. The total fluorescence intensity is measured as the sum of the fluorescence intensity inside a region of interest defined by the boundary of the cell. The data points represent the average value, and the error bars represent the standard deviation from 5 to 6 cells. Only one among every fifth data point is shown for improving visibility. (b) A representative plot showing the fluorescence intensity across the centerline (dashed white line in the inset, parallel to the electric field) of the cells shown in the inset at the time corresponding to the resealing time of the cell membrane. The point 0 corresponds to the first point on the cell from the side of the cathode, which emits a fluorescence intensity signal, and 1 corresponds to the last point, which emits a fluorescence intensity signal. One electric pulse of 800 V/cm with a duration of 500 μs is applied to obtain this data. The scale bars represent 10 μm. (c) A schematic showing the difference between permeabilized region (dashed lines) and pores (white circles) present within the permeabilized region.

inside cells is observed with respect to background noise. The transient increase of I_{Total} for the control cells and the cells treated with latrunculin B at room temperature are plotted in Fig. 2(a). For brevity, we refer to cells treated with latrunculin B either as cells with disrupted actin or as treated cells in the rest of the article. Fig. 2(a) shows that the I_{Total} is higher for the treated cells compared to the control cells. This indicates that the treated cells take up more PI compared to the control cells. In addition, the fluorescence intensity along the centerline of representative control and treated cell (displayed in inset of Fig. 2(b)) parallel to the direction of the electric field is plotted in Fig. 2(b). The centerline fluorescence profiles for all the cells studied at this condition is provided in the Supplementary information (Figs. S4 and S5). Inset from Fig. 2(b) shows that while the uptake of PI is symmetric in the control cells, it is asymmetric in the cells with disrupted actin. In the cells with disrupted actin, there is almost a two-times higher fluorescence intensity that is emitted at the pole of the cell facing the positive electrode compared to the pole facing the negative electrode. Mobility of nucleic acids, which are responsible for fluorescence signal emitted when PI enters the cell, is known to increase up to an order of magnitude on the disruption of actin networks inside the cell [52]. The increased fluorescence intensity on the pole facing the anode could be due to the easier migration of the negatively charged nucleic acids inside the treated cells towards the positive electrode when an electric field is applied.

Transport of PI to cells is dependent on the permeabilized area of the cell membrane and the resealing time of the membrane [50]. The membrane becomes permeable in the regions, where the transmembrane voltage exceeds a critical value, and these regions are called "permeabilized areas". The increased permeability within the permeabilized area is thought to be due to the presence of pores, as shown in Fig. 2(c). For brevity, we refer to the sum area of the pores on the membrane as the "pore area" in the rest of the article. Consider a cell of volume V placed in an electroporation buffer containing propidium ions of concentration c_e and exposed to an electric field. Upon exposure, the permeability of the cell membrane increases such that the pore area is A_{p0}. Once the cell membrane is permeable, the propidium ions enter the cell and bind to the nucleic acids and form a fluorescent species with the concentration [PIB]. If d is the thickness of the cell membrane, D is the diffusion coefficient of propidium ions in the electroporation buffer, and τ is the time scale of resealing of the cell membrane, the concentration of bound propidium ions can be expressed as [50,51,53]

$$[\mathrm{PIB}] = \frac{Dc_eA_{p0}\tau}{Vd}(1 - \exp(-t/\tau)). \quad (1)$$

Assuming that the fluorescence signal emitted by bound propidium ions vary linearly with [PIB] as $I_{Total} = m \cdot [\mathrm{PIB}]$, we obtain $I_{Total} = I_{max}(1 - \exp(-t/\tau))$, where $I_{max} = (mDc_eA_{p0}\tau)/(Vd)$. m is the proportionality constant that relates the concentration of bound propidium ions to the fluorescence intensity measured by the imaging system, and I_{max} is the plateau of fluorescence intensity emitted by the cell after electroporation in the presence of PI. Eq. (1) is then fitted to the temporal evolution of fluorescence intensity obtained from the image analysis using *lsqcurvefit()* function in Matlab® to obtain I_{max} and τ as displayed in Fig. S7 (Supplementary information). It is observed that the I_{max} is ~695 ± 237 a.u. for the control cells while the treated cells display approximately three times higher I_{max} of ~1945 ± 442 a.u. The extracted resealing time τ is ~13 ± 7 s for the control cells ~8 ± 3 s for the treated cells. An additional parameter of interest is the ratio of I_{max} and τ, which is given by

$$\frac{I_{max}}{\tau} = \frac{mDc_eA_{p0}}{Vd}. \quad (2)$$

This ratio is directly proportional to the initial pore area on the cell membrane after the electric pulse and the diffusion coefficient of PI through the cell membrane, which are temperature dependent quantities. I_{max}/τ is measured to be 67 ± 45 for the control cells and 279 ± 104 for the treated cells. Assuming that the cells have a similar volume, this indicates that the average pore area is significantly larger (~4 times) for cells with disrupted actin in comparison to control cells. However, Fig. 1(b) shows that the propidium ions can enter through a larger part of the cell membrane in the control cells compared to the treated cells. There are three possibilities to explain the higher uptake of PI in the treated cells despite the lower permeabilized portion of the cell membrane: *(i)* the treated cells have more pores within the permeabilized area than in the control cells leading to higher pore density; *(ii)* the size of the pores is larger in the treated cells than in the control cells; *(iii)* or a combination of both.

3.2. Temperature-dependent uptake of propidium iodide into CHO cells with intact and disrupted actin networks

One of the most accepted descriptions of the electropermeabilization of cell membranes as a response to the applied electric field is the nucleation theory of electroporation [17]. According to this theory, the rate of formation and closure of transmembrane pores is dependent on the temperature of the cell membrane [17,21,26]. The temperature-dependent rate of the creation and closure of the pores are governed by activation energy barriers [16]. Hence, the pore area and the lifetime of permeability of the cell membrane depend on the temperature. An experiment which uses the temperature dependence of the pore area and the lifetime of permeability hence allows us to measure the energy barrier of pore formation [21].

To study the energetics of the electropores and its dependence on the internal architecture of the actin networks, we perform experiments studying the uptake of PI into CHO cells (both control cells and cells treated by latrunculin B) at different temperatures ranging from 11 °C to 37 °C. We make the following observations from the temperature-dependent PI uptake experiments. As seen in Fig. 3(a) and (b), control cells and treated cells display a higher fluorescence signal at 37 °C compared to at 11 °C, implying more transport of propidium ions at the higher temperature. By fitting the temporal fluorescence intensity data from control cells and treated cells, we obtain I_{max} and τ at different temperatures presented in the Fig. 4(a) and (b). We found that I_{max} increases systematically for the control cells while the increase is less pronounced in the treated cells (see Fig. 4(a)). As shown in this figure, the I_{max} is almost five times higher at 11 °C while approximately three times higher at 37 °C for cells with disrupted actin compared to the control cells. At the same time, Fig. 4(b) shows that τ does not have any noticeable dependence on the temperature of the cells.

The higher fluorescence intensity from the treated cells compared to the control cells can be attributed to a higher pore area in the cells with disrupted actin networks after electroporation. The nucleation theory of electroporation describes the formation of the electropores within the membrane. The rate of formation of electropores depends on a nucleation free energy barrier governed by the transition of an intact bilayer to a hydrophilic pore, through an unstable hydrophobic pore configuration [16,17]. If the effective energy barrier of pore formation within the cell membrane is E^*, the rate of formation is $\dot{n}_0 = \nu S/a_0 \exp(-E^*/k_B T)$ where k_B is the Boltzmann constant, ν is the attempt rate frequency, S is the permeabilized area, a_0 is the area per lipid molecule and T is the temperature [16,21]. If the effective area of a single pore is a_p, and the pores form for a duration t_{pore}, the accumulated pore area is

$$A_{p0} = \frac{\nu S}{a_0} \exp(-E^*/k_B T) t_{pore} a_p. \tag{3}$$

Combining the Eq. (2) with the Eq. (3), we arrive at,

$$\frac{I_{max}}{\tau} = \left(\frac{m c_e S a_p t_{pore}}{V d a_0}\right) \cdot (D\nu) \exp(-E^*/k_B T). \tag{4}$$

Taking logarithm on both sides, we arrive at,

$$\ln\left(\frac{I_{max}}{\tau}\right) = \ln\left(\frac{m c_e S a_p t_{pore}}{V d a_0}\right) + \ln(D\nu) - \frac{E^*}{k_B T}. \tag{5}$$

Eq. (5) provides us a way to estimate the nucleation barrier for the pore formation within the cell membrane by the dependence of $\ln(I_{max}/\tau)$ versus temperature. We demonstrate that $\ln(I_{max}/\tau)$ is significantly higher for the cells with disrupted actin compared to the control cells at all the temperatures in Fig. 4(c). A second observation is that $\ln(I_{max}/\tau)$ increases with temperature for both the control and the cells with disrupted actin. The increase in $\ln(I_{max}/\tau)$ with temperature is more pronounced for the control cells compared to the treated cells. This effect indicates that the increase in pore area in the control cells with temperature is higher in comparison to that of the treated cells. Assuming that the duration for which electropores form is independent of the assembly of the actin networks, we infer that the rate of pore formation is higher in the treated cells compared to the control cells. Since the temperature dependence of the diffusion coefficient is independent of the structure of actin networks inside the cells, we attribute the difference in the temperature dependence of $\ln(I_{max}/\tau)$ to the

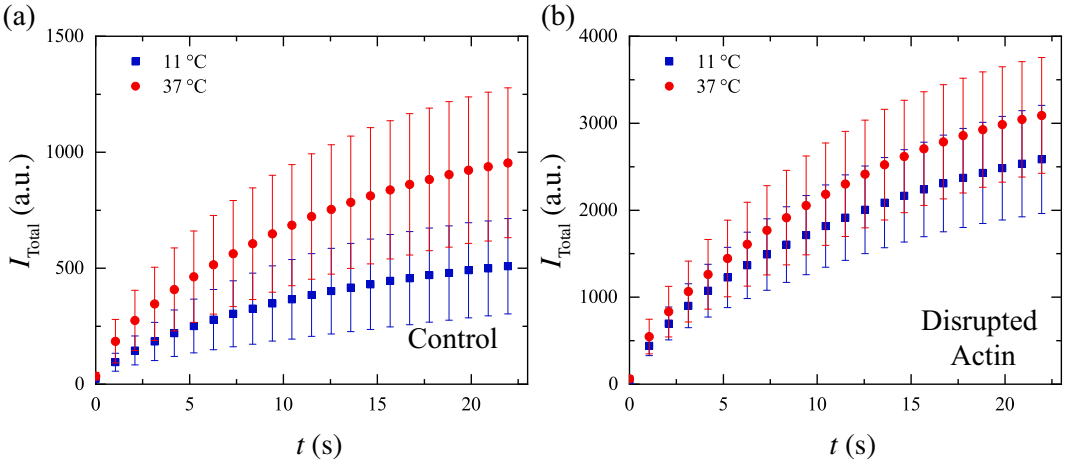

Fig. 3. Temperature dependence of I_{Total} for (a) control cells and (b) cells with disrupted actin. Data for 11°C and 37°C are shown in this figure. Only one among every fifteenth data point of the time series is shown for better clarity of the data. The symbols represent the average value, and the error bars represent the standard deviation over measurements from 4 to 7 cells. One electric pulse of 800 V/cm with a duration of 500 μs is applied to obtain this data.

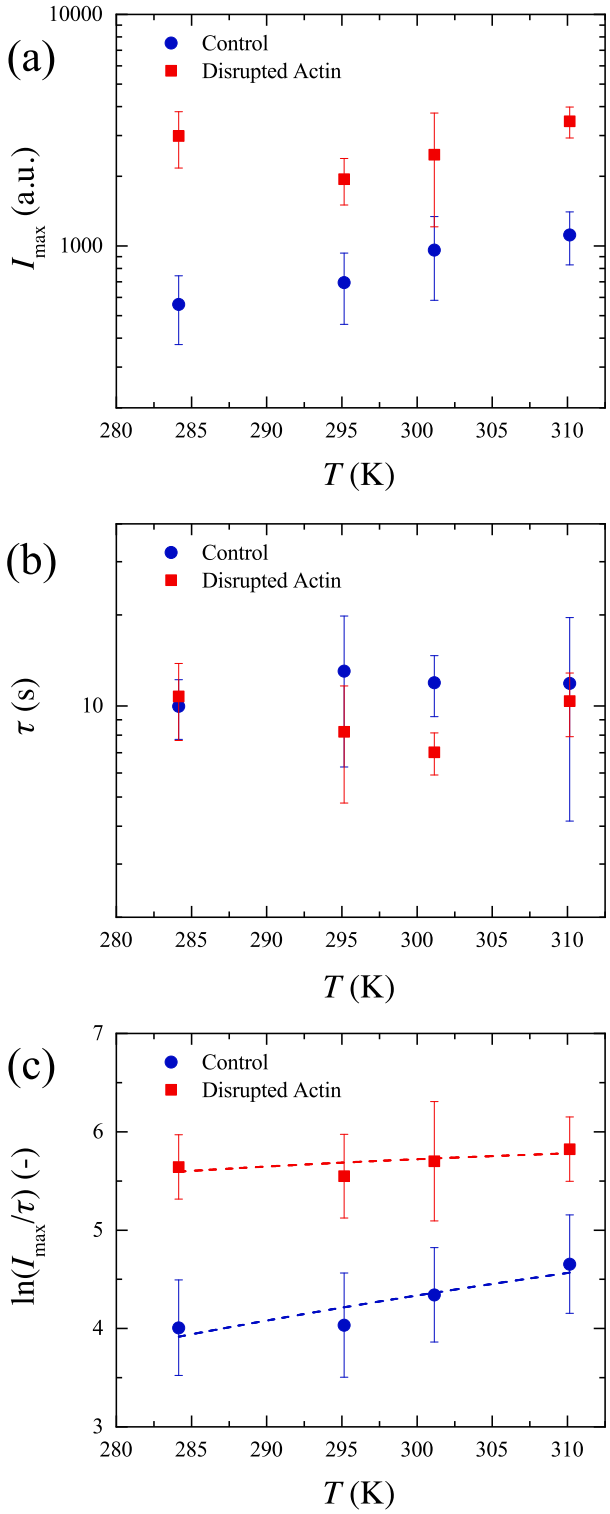

Fig. 4. (a) Dependence of the plateau fluorescence intensity I_{max} on temperature. (b) Dependence of the resealing time, τ on temperature. (c) Dependence of $\ln(I_{max}/\tau)$ on temperature. The solid symbols represent average value, and the error bars represent standard deviation over 4 to 7 cells. The dashed lines correspond to the best fit of the experimental data with Eq. (5). One electric pulse of 800 V/cm with a duration of 500 μs is applied to obtain this data.

differences in the energy barrier of pore formation in the cell membrane for the cells. Based on the temperature dependence of $\ln(I_{max}/\tau)$, we infer that the energy barrier of pore formation for the treated cells is lower than that of control cells. This hypothesis is consistent with the observation that the treated cells have a higher uptake of propidium ions in comparison to the control cells. We obtain a rough estimate of the energy barriers by fitting the experimental data with Eq. (5) after assuming diffusion coefficient and attempt rate frequency to be independent of temperature as seen in Fig. 4(c). The estimate suggests an energy barrier for pore formation of $\sim 7 \pm 2\ k_B T$ for control cells and $\sim 2 \pm 1\ k_B T$ for the treated cells. Note that the energy barriers are estimated in the presence of an applied electric field.

In addition to the experiments with an applied electric field intensity of 800 V/cm, we also performed the same experiment at lower applied electric fields. For the imaging settings that we use, the fluorescence intensity that we observe at an applied field intensity of 500 V/cm is significantly lower than that at 800 V/cm. However, the fluorescence intensity is not sufficient enough to extract any reliable information through the fitting of the experimental data. Similarly, at an applied electric field of 600 V/cm, despite post pulse diffusion being the primary contributor to the uptake of molecules, a lower uptake is observed compared to the same experiment performed at 800 V/cm. The extracted I_{max}, τ and I_{max}/τ for the molecular uptake experiment at different temperatures performed at 600 V/cm are provided in the Supplementary information (Fig. S9). Also, similar to the molecular uptake experiments performed at 800 V/cm, cells with disrupted actin show a higher uptake compared to control cells without a notable change in resealing time. The dependence of $\ln(I_{max}/\tau)$ on temperature is also similar to that at 800 V/cm, with the control cells exhibiting a stronger dependence of $\ln(I_{max}/\tau)$ on temperature compared to the cells with disrupted actin. In summary, the results at 600 V/cm are consistent with the observations at 800 V/cm.

3.3. Effect of concentration of the propidium iodide on cellular uptake during electroporation at room temperature

We perform experiments with different concentrations of PI ranging from 50 μM to 125 μM for the control cells and from 25 μM to 100 μM for the treated cells at room temperature (22 °C) to study the dependence of PI uptake on the external concentration of PI. These concentrations provide sufficient fluorescence intensity inside the cell during electroporation in comparison to the background noise and do not exceed the saturation value for pixels in the imaging sensor. Fig. 5 shows the results of the experiments demonstrating the dependence of the uptake of the propidium ions on the external concentration of PI, c_e. Fig. 5(a) displays that the I_{max} increases with concentration for control and treated cells as expected. We also observe that the uptake of PI is significantly higher in the treated cells in comparison to the control cells for the range of the tested concentrations. In other words, it is possible to deliver the same dosage of propidium ions to the treated cells with a lower external concentration of PI compared to the control cells.

The Eq. (2) states that I_{max}/τ increases linearly with the concentration of PI outside, c_e. The slope of a plot between I_{max}/τ and c_e can be determined as

$$\frac{d}{dc_e}\left(\frac{I_{max}}{\tau}\right) = \frac{mDA_{p0}\tau}{Vd}. \quad (6)$$

Eq. (6) shows that the slope of the plot between I_{max}/τ and c_e is directly proportional to A_{p0}. Hence, the dependence of uptake of PI on the external concentration of PI allows us to determine the ratio of the pore area between the control and the treated cells. The dependence of I_{max}/τ with c_e is plotted in Fig. 5(c). The plot shows that I_{max}/τ increases with c_e for both the control and the treated cells. It can be observed that the slope of increase of I_{max}/τ with c_e is lower for the control cells in comparison to the treated cells as expected from Eq. (6). The slopes (right hand side of Eq. (6)) are estimated by linear fitting (to Eq. (2)) using OriginPro, after fixing the y-intercept of the fit at zero. The corresponding values for the slope for control cells and cells with disrupted actin are $1.23 \pm 0.22\ M^{-1}$ and $3.38 \pm 0.35\ M^{-1}$ respectively. From

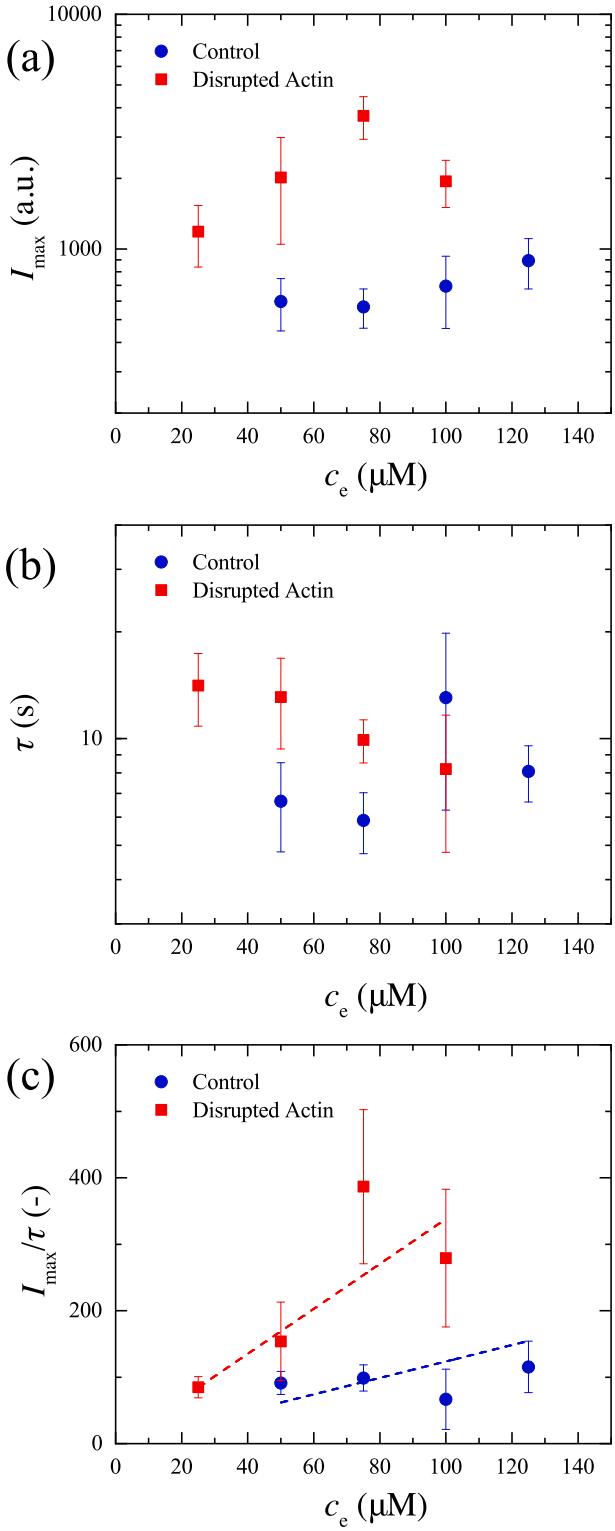

Fig. 5. (a) Dependence of plateau fluorescence intensity I_{max} on c_e. (b) Dependence of resealing time, τ on c_e. (c) Dependence of I_{max}/τ on c_e. The solid symbols represent the average value and the error bars represent the standard deviation over 5 to 8 cells. The dashed lines represent best linear fit of the data with Eq. (2) used to estimate the right hand side of Eq. (6). One electric pulse of 800 V/cm with a duration of 500 μs is applied to obtain this data. This data is obtained at room temperature.

the ratio of the slopes, it can be inferred that the pore area is ~2.7 times higher in cells with disrupted actin in comparison to control cells, reaffirming the inference made in the Section 3.1 that the estimated pore area can be ~4 times higher in cells with disrupted actin compared to control cells.

4. Discussion

Our results indicate that actin networks are involved in the electropore formation in living cells. Previous experiments have shown that the incorporation of actin network into giant unilamellar vesicles (GUVs) resulted in a higher molecular uptake through the lipid membrane due to the resulting longer resealing time compared to the empty GUVs [36]. In our study, the estimated average resealing time at room temperature of the control cells is ~ 60% longer compared to the cells treated with latrunculin B; however, despite their shorter resealing time, the treated cells exhibit more PI uptake. This suggests that the total area of the membrane pores, which allow the transport of the propidium ions, is higher in the treated cells. Since a more substantial part of the cell membrane is electropermeabilized in the control cells compared to the treated cells, this further suggests that a large amount of pore area resides within a smaller permeabilized area for the treated cells.

The electropermeabilization of the cell membrane is typically described by the formation of metastable pores on the cell membrane, which is facilitated by the transmembrane voltage induced by the applied electric field [17]. Analytical calculations for spheroidal cells show that the induced V_m is a function of the cell size, the shape, and the orientation, and reaches higher absolute values in cells, which are larger and/or elongated having their major axis aligned with the direction of the electric field [54,55]. The permeabilized area is hence expected to be higher in the control cells, which are larger and elongated, compared to the more spherical treated cells. However, we observe higher PI uptake in the treated cells. Higher uptake thus cannot be attributed to a larger permeabilized area or longer resealing time but a higher number and/or size of the pores within the permeabilized region. The latter can be attributed to a higher rate of pore creation in the treated cells, as detailed below.

According to the nucleation theory, the rate of the pore formation depends on the number of possible pore nucleation sites, the energy barrier of pore formation, and the temperature. Our experiments at different temperatures between 11 °C and 37 °C indicate that the disruption of actin filament reduces the energy barrier of pore formation, thereby increasing the rate of pore formation compared to control cells. The energy barrier of pore formation, E^* can be considered as a sum of two components: *(i)* the energy barrier in the absence of electric field E_0, which depends on the membrane interfacial tension (Γ), and the pore edge tension (γ); and *(ii)* the decrease in the energy barrier due to induced V_m. The theoretical models of electroporation typically assume the following relation:

$$E^* = E_0 - BV_m^2. \tag{7}$$

In the above relation, B is a proportionality constant [18,21]. As discussed above, analytical calculations demonstrate that V_m should be higher in the elongated cells; in our case, the control cells. This means that the lower energy barrier for pore formation in the treated cells, which we deduce from our analysis, is not due to the higher V_m induced on the treated cells. We corroborate this conclusion further by performing numerical calculations (see Supplementary information for details of the numerical calculations) of the V_m on cylindrical cells with different sizes and orientation (Fig. 6(a)), as depicted in Fig. 6 as well as on spheroidal cells as reported in the Supplementary information (Fig. S13). Fig. 6(b) shows the time course of the V_m at the two poles of each cell when the cells are exposed to a 500 μs, 800 V/cm pulse. Regardless of the cell geometry, V_m reaches a peak value of ~ 0.8 V upon which it

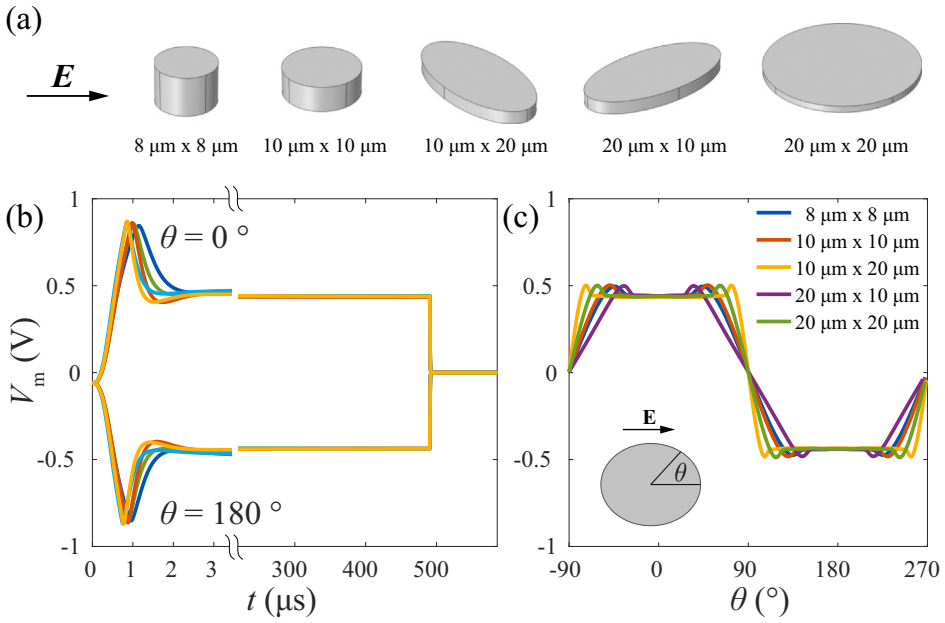

Fig. 6. Calculations of the induced transmembrane voltage for the cylindrical cells having volumes that mimic our experimental cases. The details of the numerical calculations are provided in the Supplementary information (see Section S7). (a) 3D representation of the cell geometry considered. (b) Time course of the transmembrane voltage at the anodic and the cathodic pole of the cell(at $\theta = 0^{\circ}$ and $\theta = 180^{\circ}$). (c) Profile of the induced transmembrane voltage along the cell membrane at the end of a 500 μs, 800 V/cm pulse (identical to the experimental conditions). θ is the angle between the point on the membrane and the electric field E (see inset).

decreases and stabilizes at ~ 0.5 V. This decrease, also referred to as "electrical membrane breakdown" is due to an increase in the membrane conductivity caused by the formation of pores in the membrane. Since the pore creation rate is proportional to

$$\dot{n}_0 = \exp\left(-\frac{E_0}{k_B T} + \frac{BV_m^2}{k_B T}\right) \tag{8}$$

almost all the pores form in the membrane around the time of electrical breakdown when the V_m reaches its highest absolute value. Since the highest V_m practically does not depend on cell geometry, we exclude V_m as a possible source of the reduced energy barrier for pore formation in cells with disrupted actin filaments. To strengthen this conclusion further, we show numerical calculations in the Supplementary material (Fig. S12) that by applying a lower electric field of 600 V/cm, the peak V_m is still about 0.8 V. Accordingly, we deduce similar values of the pore creation energy from experimental measurements at 600 V/cm (Fig. S9). Despite the similar values of pore creation energy at 600 V/cm, we observe a lower uptake of propidium ions to the cell compared to experiments at 800 V/cm. This can be attributed to the lower permeabilized area that is formed at lower voltages [29]. In Fig. 6, we show calculations for cells with cylindrical shapes, keeping the cell volume constant, which we consider as the most representative for our experimental conditions. However, in Fig. S13 (Supplementary information), we show that similar results are obtained for spheroidal cells with different volumes, further confirming that the time course of V_m is not highly dependent on the cell shape and size. We obtain the same conclusions by performing propidium uptake experiments on cells with intact actin networks, but a roughly spherical shape (Supplementary information Section S1). We show that the propidium uptake of CHO cells with a roughly spherical shape and intact actin networks have similar uptake profiles as our control cells, and a much lower uptake compared to cells treated by latrunculin (Fig. S1 and Fig. S2). In addition, we also show that disruption of actin with lower concentration (0.25 μM) still results in higher uptake of propidium compared to control cells, but lower compared to cells treated by latrunculin (0.5 μM), which provides clear evidence that the increased uptake that we observe is due to the disruption of actin.

Apart from V_m, the energy barrier of pore formation is also dependent on the membrane interfacial tension (Γ), and the pore edge tension (γ) [56,57]. The free energy difference E between a defect-free lipid bilayer and one with a single hydrophilic pore of radius r_p is theoretically described as $E = 2\pi r_p \gamma - \pi r_p^2 \Gamma$ [56]. The interfacial tension promotes the expansion of the pores while the edge tension works to close it. In the nucleation theory of electroporation, the energy barrier E^* is defined as the energy of the hydrophilic/hydrophobic pore when a hydrophobic pore transitions to a hydrophilic pore, which is theorized to happen at a pore radius of ~ 0.5 nm. The contribution of surface tension to the free energy is negligible in comparison to that of edge tension for pores in size range of few nanometers, which are theorized to form during electroporation [57]. Hence, we discuss the influence of actin networks on the edge tension below.

As long-lived micron-sized pores have to be created for measuring edge tension, the reported values of measured edge tension were only obtained from experiments utilizing GUVs [58–61]. Since there are currently no visualizations of electropores in the cell membrane, a direct estimate of the edge tension is not available for the cell membranes with intact actin networks. Considering that the essence of edge tension is the energy required to bend the lipid bilayer at the rim of the pore, we can make estimates of edge tension from measurements of bending modulus (κ) of the cell membrane [27,62]. Assuming that the transmembrane pore is much larger than the membrane thickness ($d = 5$ nm), γ can be related to the κ as $\gamma \sim \pi\kappa/2d$; which means that the edge tension (γ) is directly proportional to the bending modulus (κ) [27]. The measurement of bending modulus in HeLa cells has suggested that the bending modulus is approximately ten times higher in the presence of a cortical actin network compared to a bleb devoid of actin networks [63]. Similarly, experiments show that elastic modulus, a property often related to bending modulus, is shown to be halved when actin networks are depolymerized [64,65]. A lower bending modulus or a lower edge tension means that the pore energy is lower for the treated cells compared to the control cells. Hence, a lower energy barrier of pore formation for the treated cells, which we measure, could be attributed to a reduced bending modulus of the cell membrane when the actin networks are disrupted. As seen from Eq. (8), a lower energy barrier of electroporation is associated with an increased number of pores in the membrane, which is consistent with our estimate that total area occupied by the pores in the membrane of the treated cells is higher than the control cells. However, we cannot completely exclude the possibility that the average size of individual pores is also higher in the treated cells. For instance, studies on cell fusion have proposed that actin networks restrict the growth of fusion pores and that the fusion pores are accompanied by disassembly of the actin cortex under the

pores [66], and theoretical models have suggested that cytoskeletal networks may stabilize the membrane against pore growth [67].

5. Conclusion

The role of actin in electroporation is studied in living cells by monitoring the uptake of propidium iodide to CHO cells. The disruption of actin networks causes higher uptake during electroporation. The uptake of propidium iodide to cells depend on the temperature in the range studied (11 °C to 37 °C), and uptake of propidium iodide increases with increasing temperature. The cells with disrupted actin networks show a weaker temperature dependence compared to the control cells. These results are analyzed using the nucleation theory of electroporation, and we conclude that the cells with disrupted actin networks have a reduced energy barrier of electropore formation. To approach towards better electroporation models, we thus suggest to consider the contribution of actin networks in the molecular description of electropore formation kinetics. In addition, it will be fruitful to test the effect of actin disruption on the uptake of biologically relevant molecules (e.g. siRNA and DNA) in the future studies [47,68].

CRediT authorship contribution statement

1. Aswin Muralidharan: Conceptualization, Methodology, Software, Validation, Formal analysis, Investigation, Data curation, Writing – original draft, Visualization, Project administration.
2. Lea Rems: Software, Formal analysis, Investigation, Writing – review and editing, Visualization.
3. Michiel T. Kreutzer: Supervision.
4. Pouyan E. Boukany: Conceptualization, Writing – review and editing, Supervision, Project administration, Funding acquisition.

Supplementary data to this article can be found online at https://doi.org/10.1016/j.bbamem.2020.183468.

Declaration of competing interest

The authors declare that they have no known competing financial interests or personal relationships that could have appeared to influence the work reported in this paper.

Acknowledgments

We thank Georg Pesch and Zaid Rahman for the critical reading of the manuscript. We acknowledge the funding from the European Research Council (ERC) under the European Union's Horizon 2020 research and innovation programme (grant agreement no. 819424).

References

[1] H. Lodish, A. Berk, C.A. Kaiser, M. Krieger, M.P. Scott, A. Bretscher, H. Ploegh, P. Matsudaira, et al., Molecular Cell Biology, Macmillan, 2008.
[2] D.A. Fletcher, R.D. Mullins, Cell mechanics and the cytoskeleton, Nature 463 (7280) (2010) 485.
[3] M.P. Stewart, R. Langer, K.F. Jensen, Intracellular delivery by membrane disruption: mechanisms, strategies, and concepts, Chem. Rev. 118 (16) (2018) 7409–7531.
[4] K. Kinosita Jr., T.Y. Tsong, Formation and resealing of pores of controlled sizes in human erythrocyte membrane, Nature 268 (5619) (1977) 438.
[5] T. Kotnik, L. Rems, M. Tarek, D. Miklavčič, Membrane electroporation and electropermeabilization: mechanisms and models, Annu. Rev. Biophys. 48 (2019) 63–91.
[6] L.C. Heller, R. Heller, In vivo electroporation for gene therapy, Hum. Gene Ther. 17 (9) (2006) 890–897.
[7] D. Miklavčič, B. Mali, B. Kos, R. Heller, G. Serša, Electrochemotherapy: from the drawing board into medical practice, Biomed. Eng. Online 13 (1) (2014) 29.
[8] M.L. Yarmush, A. Golberg, G. Serša, T. Kotnik, D. Miklavčič, Electroporation-based technologies for medicine: principles, applications, and challenges, Annu. Rev. Biomed. Eng. 16 (2014) 295–320.
[9] B. Geboers, H.J. Scheffer, P.M. Graybill, A.H. Ruarus, S. Nieuwenhuizen, R.S. Puijk, P.M. van den Tol, R.V. Davalos, B. Rubinsky, T.D. de Gruijl, et al., High-voltage electrical pulses in oncology: irreversible electroporation, electrochemotherapy, gene electrotransfer, electrofusion, and electroimmunotherapy, Radiology 295 (2020) 254–272 192190.
[10] C.L. Trimble, M.P. Morrow, K.A. Kraynyak, X. Shen, M. Dallas, J. Yan, L. Edwards, R.L. Parker, L. Denny, M. Giffear, et al., Safety, efficacy, and immunogenicity of vgx-3100, a therapeutic synthetic DNA vaccine targeting human papillomavirus 16 and 18 e6 and e7 proteins for cervical intraepithelial neoplasia 2/3: a randomised, double-blind, placebo-controlled phase 2b trial, Lancet 386 (10008) (2015) 2078–2088.
[11] K. Modjarrad, C.C. Roberts, K.T. Mills, A.R. Castellano, K. Paolino, K. Muthumani, E.L. Reuschel, M.L. Robb, T. Racine, M.-d. Oh, et al., Safety and immunogenicity of an anti-middle east respiratory syndrome coronavirus DNA vaccine: a phase 1, open-label, single-arm, dose-escalation trial, Lancet Infect. Dis. 19 (9) (2019) 1013–1022.
[12] E. Maor, A. Sugrue, C. Witt, V.R. Vaidya, C.V. DeSimone, S.J. Asirvatham, S. Kapa, Pulsed electric fields for cardiac ablation and beyond: a state-of-the-art review, Heart Rhythm. 16 (7) (2019) 1112–1120.
[13] J. Teissie, M. Golzio, M. Rols, Mechanisms of cell membrane electropermeabilization: a minireview of our present (lack of?) knowledge, Biochimica et Biophysica Acta (BBA)-General Subjects 1724 (3) (2005) 270–280.
[14] W. Krassowska, P.D. Filev, Modeling electroporation in a single cell, Biophys. J. 92 (2) (2007) 404–417.
[15] I. Abidor, V. Arakelyan, L. Chernomordik, Y.A. Chizmadzhev, V. Pastushenko, M. Tarasevich, Electric breakdown of bilayer lipid membranes: I. the main experimental facts and their qualitative discussion, J. Electroanal. Chem. Interfacial Electrochem. 104 (1979) 37–52.
[16] R.W. Glaser, S.L. Leikin, L.V. Chernomordik, V.F. Pastushenko, A.I. Sokirko, Reversible electrical breakdown of lipid bilayers: formation and evolution of pores, Biochimica et Biophysica Acta (BBA)-Biomembranes 940 (2) (1988) 275–287.
[17] J.C. Weaver, Y.A. Chizmadzhev, Theory of electroporation: a review, Bioelectrochem. Bioenerg. 41 (2) (1996) 135–160.
[18] Z. Vasilkoski, A.T. Esser, T. Gowrishankar, J.C. Weaver, Membrane electroporation: the absolute rate equation and nanosecond time scale pore creation, Phys. Rev. E 74 (2) (2006) 021904.
[19] D.L. Perrier, L. Rems, P.E. Boukany, Lipid vesicles in pulsed electric fields: fundamental principles of the membrane response and its biomedical applications, Adv. Colloid Interf. Sci. 249 (2017) 248–271.
[20] J.T. Sengel, M.I. Wallace, Imaging the dynamics of individual electropores, Proc. Natl. Acad. Sci. 113 (19) (2016) 5281–5286.
[21] J.T. Sengel, M.I. Wallace, Measuring the potential energy barrier to lipid bilayer electroporation, Philosophical Transactions of the Royal Society B: Biological Sciences 372 (1726) (2017) 20160227.
[22] T. Portet, F.C. i Febrer, J.-M. Escoffre, C. Favard, M.-P. Rols, D.S. Dean, Visualization of membrane loss during the shrinkage of giant vesicles under electropulsation, Biophys. J. 96 (10) (2009) 4109–4121.
[23] K.A. Riske, R. Dimova, Electro-deformation and poration of giant vesicles viewed with high temporal resolution, Biophys. J. 88 (2) (2005) 1143–1155.
[24] M. Tarek, Membrane electroporation: a molecular dynamics simulation, Biophys. J. 88 (6) (2005) 4045–4053.
[25] D.P. Tieleman, The molecular basis of electroporation, BMC Biochem. 5 (1) (2004) 10.
[26] A.K. Majhi, S. Kanchi, V. Venkataraman, K. Ayappa, P.K. Maiti, Estimation of activation energy for electroporation and pore growth rate in liquid crystalline and gel phases of lipid bilayers using molecular dynamics simulations, Soft Matter 11 (44) (2015) 8632–8640.
[27] J. Wohlert, W.K. den Otter, O. Edholm, W.J. Briels, Free energy of a trans-membrane pore calculated from atomistic molecular dynamics simulations, J. Chem. Phys. 124 (15) (2006) 154905.
[28] C.L. Ting, N. Awasthi, M. Müller, J.S. Hub, Metastable prepores in tension-free lipid bilayers, Phys. Rev. Lett. 120 (12) (2018) 128103.
[29] M.-P. Rols, J. Teissie, Electropermeabilization of mammalian cells. Quantitative analysis of the phenomenon, Biophys. J. 58 (5) (1990) 1089–1098.
[30] R. Shirakashi, V.L. Sukhorukov, I. Tanasawa, U. Zimmermann, Measurement of the permeability and resealing time constant of the electroporated mammalian cell membranes, Int. J. Heat Mass Transf. 47 (21) (2004) 4517–4524.
[31] E. Tekle, R. Astumian, W. Friauf, P. Chock, Asymmetric pore distribution and loss of membrane lipid in electroporated dopc vesicles, Biophys. J. 81 (2) (2001) 960–968.
[32] S. Sachdev, A. Muralidharan, D.K. Choudhary, D.L. Perrier, L. Rems, M.T. Kreutzer, P.E. Boukany, DNA translocation to giant unilamellar vesicles during electroporation is independent of DNA size, Soft Matter 15 (45) (2019) 9187–9194.
[33] R.L. Knorr, M. Staykova, R.S. Gracià, R. Dimova, Wrinkling and electroporation of giant vesicles in the gel phase, Soft Matter 6 (9) (2010) 1990–1996.
[34] D.L. Perrier, L. Rems, M.T. Kreutzer, P.E. Boukany, The role of gel-phase domains in electroporation of vesicles, Sci. Rep. 8 (1) (2018) 1–10.
[35] I. van Uitert, S. Le Gac, A. van den Berg, The influence of different membrane components on the electrical stability of bilayer lipid membranes, Biochimica et Biophysica Acta (BBA)-Biomembranes 1798 (1) (2010) 21–31.
[36] D.L. Perrier, A. Vahid, V. Kathavi, L. Stam, L. Rems, Y. Mulla, A. Muralidharan, G.H. Koenderink, M.T. Kreutzer, P.E. Boukany, Response of an actin network in vesicles under electric pulses, Sci. Rep. 9 (1) (2019) 8151.
[37] M.-P. Rols, J. Teissié, Experimental evidence for the involvement of the cytoskeleton in mammalian cell electropermeabilization, Biochimica et Biophysica Acta (BBA)-Biomembranes 1111 (1) (1992) 45–50.
[38] J. Teissié, M.-P. Rols, Manipulation of cell cytoskeleton affects the lifetime of cell membrane electropermeabilization, Ann. N. Y. Acad. Sci. 720 (1) (1994) 98–110.

[39] C. Blangero, M. Rols, J. Teissie, Cytoskeletal reorganization during electric-field-induced fusion of chinese hamster ovary cells grown in monolayers, Biochimica et Biophysica Acta (BBA)-Biomembranes 981 (2) (1989) 295–302.
[40] C. Kanthou, S. Kranjc, G. Sersa, G. Tozer, A. Zupanic, M. Cemazar, The endothelial cytoskeleton as a target of electroporation-based therapies, Mol. Cancer Ther. 5 (12) (2006) 3145–3152.
[41] L. Chopinet, C. Roduit, M.-P. Rols, E. Dague, Destabilization induced by electropermeabilization analyzed by atomic force microscopy, Biochimica et Biophysica Acta (BBA)-Biomembranes 1828 (9) (2013) 2223–2229.
[42] J. Dinic, P. Ashrafzadeh, I. Parmryd, Actin filaments attachment at the plasma membrane in live cells cause the formation of ordered lipid domains, Biochimica et Biophysica Acta (BBA)-Biomembranes 1828 (3) (2013) 1102–1111.
[43] R. Reigada, Electroporation of heterogeneous lipid membranes, Biochimica et Biophysica Acta (BBA)-Biomembranes 1838 (3) (2014) 814–821.
[44] P.M. Graybill, R.V. Davalos, Cytoskeletal disruption after electroporation and its significance to pulsed electric field therapies, Cancers 12 (5) (2020) 1132.
[45] H.B. Kim, S. Lee, J.H. Chung, S.N. Kim, C.K. Sung, K.Y. Baik, Effects of actin cytoskeleton disruption on electroporation in vitro, Appl. Biochem. Biotechnol. (2020) 1–17.
[46] A.T. Esser, K.C. Smith, T. Gowrishankar, Z. Vasilkoski, J.C. Weaver, Mechanisms for the intracellular manipulation of organelles by conventional electroporation, Biophys. J. 98 (11) (2010) 2506–2514.
[47] C. Rosazza, J.-M. Escoffre, A. Zumbusch, M.-P. Rols, The actin cytoskeleton has an active role in the electrotransfer of plasmid DNA in mammalian cells, Mol. Ther. 19 (5) (2011) 913–921.
[48] T.D. Pollard, W.C. Earnshaw, J. Lippincott-Schwartz, G. Johnson, Cell Biology, Elsevier Health Sciences (2016) 575–591.
[49] T.B. Napotnik, D. Miklavčič, In vitro electroporation detection methods–an overview, Bioelectrochemistry 120 (2018) 166–182.
[50] G. Pucihar, T. Kotnik, D. Miklavčič, J. Teissié, Kinetics of transmembrane transport of small molecules into electropermeabilized cells, Biophys. J. 95 (6) (2008) 2837–2848.
[51] J. Dermol, O.N. Pakhomova, A.G. Pakhomov, D. Miklavčič, Cell electrosensitization exists only in certain electroporation buffers, PLoS One 11 (7) (2016) e0159434.
[52] E. Dauty, A. Verkman, Actin cytoskeleton as the principal determinant of size-dependent DNA mobility in cytoplasm a new barrier for non-viral gene delivery, J. Biol. Chem. 280 (9) (2005) 7823–7828.
[53] Z. Fan, H. Liu, M. Mayer, C.X. Deng, Spatiotemporally controlled single cell sonoporation, Proc. Natl. Acad. Sci. 109 (41) (2012) 16486–16491.
[54] T. Kotnik, G. Pucihar, D. Miklavčič, Induced transmembrane voltage and its correlation with electroporation-mediated molecular transport, J. Membr. Biol. 236 (1) (2010) 3–13.
[55] B. Valič, M. Golzio, M. Pavlin, A. Schatz, C. Faurie, B. Gabriel, J. Teissié, M.-P. Rols, D. Miklavčič, Effect of electric field induced transmembrane potential on spheroidal cells: theory and experiment, Eur. Biophys. J. 32 (6) (2003) 519–528.
[56] J. Litster, Stability of lipid bilayers and red blood cell membranes, Phys. Lett. A 53 (3) (1975) 193–194.
[57] J.C. Neu, W. Krassowska, Asymptotic model of electroporation, Phys. Rev. E 59 (3) (1999) 3471.
[58] O. Sandre, L. Moreaux, F. Brochard-Wyart, Dynamics of transient pores in stretched vesicles, Proc. Natl. Acad. Sci. 96 (19) (1999) 10591–10596.
[59] P.-H. Puech, N. Borghi, E. Karatekin, F. Brochard-Wyart, Line thermodynamics: adsorption at a membrane edge, Phys. Rev. Lett. 90 (12) (2003) 128304.
[60] E. Karatekin, O. Sandre, H. Guitouni, N. Borghi, P.-H. Puech, F. Brochard-Wyart, Cascades of transient pores in giant vesicles: line tension and transport, Biophys. J. 84 (3) (2003) 1734–1749.
[61] T. Portet, R. Dimova, A new method for measuring edge tensions and stability of lipid bilayers: effect of membrane composition, Biophys. J. 99 (10) (2010) 3264–3273.
[62] M.M. Kozlov, L.V. Chernomordik, Membrane tension and membrane fusion, Curr. Opin. Struct. Biol. 33 (2015) 61–67.
[63] G.T. Charras, M. Coughlin, T.J. Mitchison, L. Mahadevan, Life and times of a cellular bleb, Biophys. J. 94 (5) (2008) 1836–1853.
[64] J.-Y. Tinevez, U. Schulze, G. Salbreux, J. Roensch, J.-F. Joanny, E. Paluch, Role of cortical tension in bleb growth, Proc. Natl. Acad. Sci. 106 (44) (2009) 18581–18586.
[65] G. Salbreux, G. Charras, E. Paluch, Actin cortex mechanics and cellular morphogenesis, Trends Cell Biol. 22 (10) (2012) 536–545.
[66] A. Chen, E. Leikina, K. Melikov, B. Podbilewicz, M.M. Kozlov, L.V. Chernomordik, Fusion-pore expansion during syncytium formation is restricted by an actin network, J. Cell Sci. 121 (21) (2008) 3619–3628.
[67] W. Sung, P. Park, Dynamics of pore growth in membranes and membrane stability, Biophys. J. 73 (4) (1997) 1797–1804.
[68] S. Sachdev, S.F. Moreira, Y. Keehnen, L. Rems, M.T. Kreutzer, P.E. Boukany, DNA-membrane complex formation during electroporation is DNA size-dependent, Biochimica et Biophysica Acta (BBA)-Biomembranes 1862 (2) (2020) 183089.